This is a preprint, the final version is subject to change, of the American Mineralogist (MSA)
Cite as Authors (Year) Title. American Mineralogist, in press.
DOI: https://doi.org/10.2138/am-2020-7272

Revision 1

Ti Diffusion in Feldspar

D.J. Cherniak*, E.B. Watson
Department of Earth and Environmental Sciences
Rensselaer Polytechnic Institute
Troy, NY 12180 USA

*Corresponding author:
D.J. Cherniak
Department of Earth & Environmental Sciences
Rensselaer Polytechnic Institute
Troy, NY 12180
chernd@rpi.edu

Keywords: titanium, feldspar, diffusion, Rutherford Backscattering spectrometry

Abstract

Chemical diffusion of Ti has been measured in natural K-feldspar and plagioclase. The sources of diffusant used were TiO_2 powders or pre-annealed mixtures of TiO_2 and Al_2O_3. Experiments were run in crimped Pt capsules in air, or in sealed silica glass capsules with solid buffers (to buffer at NNO). Rutherford Backscattering Spectrometry (RBS) was used to measure Ti diffusion profiles. From these measurements, the following Arrhenius relations are obtained for diffusion normal to (001):

For oligoclase, over the temperature range 750-1050ºC:
$D_{Olig} = 6.67 \times 10^{-12} \exp(-207 \pm 31 \text{ kJ mol}^{-1}/RT) \text{ m}^2\text{sec}^{-1}$

For labradorite, over the temperature range 900-1150ºC:
$D_{Lab} = \text{of } 4.37 \times 10^{-14} \exp(-181 \pm 57 \text{ kJ mol}^{-1}/RT) \text{ m}^2\text{sec}^{-1}$

For K-feldspar, over the temperature range 800-1000ºC:
$D_{Ksp} = 3.01 \times 10^{-6} \exp(-342 \pm 47 \text{ kJ mol}^{-1}/RT) \text{ m}^2\text{sec}^{-1}$

Diffusivities for experiments buffered at NNO are similar to those run in air, and the presence of hydrous species appears to have little effect on Ti diffusion. Ti diffusion also shows little evidence of anisotropy. In plagioclase, there appears to be a dependence of Ti diffusion on An content of the feldspar, with Ti diffusing more slowly in more calcic plagioclase. This trend is similar to that observed for other cations in plagioclase, including Sr, Pb, Ba, REE, Si and Mg. In the case of Ti, an increase of 30% in An content would result in an approximate decrease in diffusivity of an order of magnitude.

These data indicate that feldspar should be moderately retentive of Ti chemical signatures, depending on feldspar composition. Ti will be more resistant to diffusional alteration than Sr. For example Ti zoning on a 50μm scale in oligoclase would be preserved at 600°C for durations of ~ 1 million years, with Sr zoning preserved only for ~70,000 years at this temperature. These

new data for a trace impurity that is relatively slow-diffusing and ubiquitous in feldspars (Hoff and Watson 2018) have the potential to extend the scope and applicability of t-T models for crustal rocks based on measurements of trace elements in feldspars.

Introduction

Feldspars are among the most abundant minerals in the earth's crust. Ti is an important trace element in feldspar, likely substituting on tetrahedral sites (e.g., Parsons et al., 2008; Peters et al., 1995). Tetrahedrally coordinated Ti in albitic alkali feldspars is an activator for cathodoluminescence (Parsons et al, 2008); fine-scale zoning in feldspars observable through CL can provide information on crystal growth and geochemical histories. Ti gradients and other small-scale compositional variations within plagioclase grains may provide insight into magma chamber dynamics and processes influencing magma transport (e.g., Singer et al, 1995; Adams et al, 2011; Salmonsen et al., 2011; Ginibre et al., 2004). Ti concentrations in feldspar may also be affected by fluid mediated processes, for example the loss of Ti during albitization of potassic feldspar (Norberg et al., 2014). Feldspars may also contain Ti-rich phases formed by exsolution (e.g. Wenk et al., 2011; Ageeva et al, 2016). Further, recent work (Hoff and Watson, 2018) has indicated that Ti concentrations in feldspar may have potential as a geothermobarometer. Characterizing diffusion of Ti in feldspar provides critical constraints on these processes, and may permit derivation of information about thermal and chemical histories from Ti distributions.

In this study, we measure Ti diffusion in K-feldspar and plagioclase, evaluating potential effects of feldspar composition, orientation, and fO_2 on Ti diffusion and consider these data with respect to diffusivities of other cations in feldspar and Ti mobilities in other mineral phases.

Experimental Procedure and Materials

Diffusion experiments were conducted on specimens of natural K-feldspar and plagioclase. The K-feldspar (Or_{93}) is from Madagascar, the albite (Or_1) is from Brazil (#135031 from the collection at the National Museum of Natural History), the oligoclase (An_{23}) is from North Carolina (kindly provided by D.S. Miller), the labradorite (An_{67}) is from Lake County, Oregon (#

135512-1 from the collection at the National Museum of Natural History), and the anorthitic feldspar (An_{93}) is from Pacaya Volcano (kindly provided by D.R. Baker). Compositional information on the feldspars is presented in Table 1. These feldspars have been used is some of our previous studies of diffusion of other elements, including Sr (Cherniak and Watson, 1992; 1994; Cherniak, 1996), Pb (Cherniak, 1995), Ba (Cherniak, 2002), REE (Cherniak, 2003a), Si (Cherniak, 2003b) and Mg (Van Orman et al., 2014). The feldspars were oriented, cut into slabs about 0.5mm thick and a few mm on a side, and polished with SiC papers, then with 0.3 μm alumina, with a final chemical polish using colloidal silica.

Ti diffusion experiments were conducted using powder sources containing TiO_2. The powder sources consisted of either dried TiO_2 powder, or mixtures of TiO_2 and Al_2O_3 powders in 3:1 or 10:1 (by wt.) ratios, ground under ethanol, dried, and heated in a Pt crucible for one day at 1250°C. Sources of diffusant were selected for use in experiments because they did not react with and degrade sample surfaces during diffusion anneals. Use of sources with differing Ti concentrations also permitted some exploration of whether there might be concentration dependence of diffusivities, albeit over a limited compositional range. Experiments were prepared by surrounding feldspar crystals with the source powders in Pt capsules and crimping capsules shut. For experiments run under buffered conditions, the Pt capsules were placed inside a silica glass ampoule with another crimped Pt capsule containing the buffer material (mixtures of Ni metal and nickel oxide powders to buffer at NNO); silica glass chips were used to physically separate the sample and buffer capsules inside the silica glass ampoule. The sample-buffer assemblies were then sealed in the silica ampoule under vacuum. An experiment was also conducted to assess the effects of the presence of hydrous species on Ti diffusion. For this experiment, the capsule was prepared as above for the buffered experiments, but with the

addition of a few mg of glycine ($C_2H_5NO_2$, which decomposes at 233°C) placed in the bottom of the silica glass ampoule before loading the buffer and sample capsules.

All experiments under 1100°C were run in one-atmosphere tube furnaces with Kanthal wire windings; experiments above 1100°C were run in a one-atmosphere horizontal tube furnace with $MoSi_2$ heating elements. Sample temperatures monitored by type K or type S (Pt-Pt10%Rh) thermocouples, for temperatures below and above 1100°C, respectively. Temperature uncertainties were ~±2°C for both thermocouple types. Experiments were quenched by removing them from the furnaces and permitting them to cool in air. The feldspar crystals were removed from capsules and cleaned ultrasonically in distilled H_2O and ethyl alcohol. SEM imaging of sample surfaces following diffusion anneals showed little evidence of residual source material remaining following cleaning. Experimental conditions are presented in Tables 2 and 3.

We performed time-series studies for both oligoclase and K feldspar in order to verify that the measured concentration profiles represent volume diffusion and are not a consequence of other phenomena such as surface reaction that might otherwise result in enhanced concentrations of the diffusing species in the near-surface region. For the time series, a set of diffusion experiments were conducted at 900°C for both feldspars.

RBS analysis

Samples from Ti diffusion experiments were analyzed with RBS, which has been used as a primary analytical method in many of our diffusion studies, including those measuring Pb, Sr, Ba and the REE diffusion in feldspars (Cherniak 2003; 2002; 1995; 1996; Cherniak and Watson, 1992; 1994), and is a well-established method for materials characterization (e.g., Jeynes and Colaux, 2016). The analytical approach used here is similar to that used in earlier studies, with $^4He^+$ incident beams at energies between 2 and 3 MeV used for analysis. In cases where different

incident beam energies were used, diffusivities obtained from depth profiles agreed within uncertainties. While we did not employ other analytical methods in this study, in other investigations of diffusion, good agreement has been found between measurements obtained by RBS and those by NRA (Cherniak, 2008) and SIMS (e.g., Cherniak et al., 2004; Cherniak, 2010; Dohmen et al., 2019; Beyer et al., 2019). In addition, we have found diffusivities measured using RBS consistent with diffusivities measured by EMPA, although not at overlapping temperatures given the differences in measureable lengthscales of diffusion profiles (e.g., Cherniak et al., 1997; Cherniak and Watson, 2001).

Spectra were converted to Ti concentration profiles by employing procedures similar to those outlined in Cherniak and Watson (1994). Depth profiles obtained from RBS analyses were fit with a model to determine the diffusion coefficient (D). Diffusion is modeled as simple one-dimensional, concentration independent diffusion in a semi-infinite medium with a source reservoir maintained at constant concentration (i.e., a complementary error function solution). The rationale for the use of this model has been discussed in previous publications (e.g., Cherniak and Watson, 1992). Diffusivities are evaluated by plotting the inverse of the error function (i.e., $erf^{-1}((C_o - C(x,t))/C_o)$ vs. depth (x) in the sample. A straight line of slope $(4Dt)^{-1/2}$ results if the data conform to a complementary error function solution. C_o, the surface concentration of diffusant, is independently determined by iteratively varying its value until the intercept of the line converges on zero. Ti surface concentrations in samples range from several hundred to a few thousand ppm. This range of concentrations is generally consistent with the solubility studies of Ti in feldspar of Hoff and Watson (2018) and Hoff (2019), and considering the comparatively low silica activities in the source materials used in the present diffusion experiments.

In Figure 1, typical diffusion profiles (1a,c) and their inversions through the error function (1b,d) are shown. The uncertainties in concentration and depth from each data point (mainly derived from counting statistics and backgrounds in the former and detector resolution in the latter) were used to evaluate the uncertainties in the diffusivities determined from the fits to the model.

Results

The results for Ti diffusion in oligoclase are plotted in figure 2 and presented in Table 2 There is little evidence of diffusional anisotropy, and Ti diffusion appears to be relatively insensitive to oxygen fugacity, as diffusivities in samples annealed in air and with a NNO buffer are similar. For diffusion normal to (001), we obtain an activation energy of 207 ± 31 kJ/mol. and pre-exponential factor of 6.67×10^{-12} m^2/s ($\log D_o = -11.18 \pm 1.41$).

Ti diffusion data for labradorite, anorthite, and albite are also shown in figure 2 and table 2. For diffusion normal to (001) in labradorite, we obtain an activation energy of 181 ± 57 kJ/mol. and pre-exponential factor of 4.37×10^{-14} m^2/s ($\log D_o = -13.36 \pm 2.32$). The activation energies for Ti diffusion in plagioclase are relatively low compared with those for diffusion of many other elements measured to date, but there is overlap within uncertainties with some measured in plagioclase, including Sr and Ca (e.g., Cherniak, 2010).

We have one data point each for anorthite and albite, but there is a clear trend of increased diffusivities for more sodic plagioclase, which has also been observed for other cations, including Sr (Cherniak and Watson, 1992; 1994; Giletti and Casserly, 1994), Pb (Cherniak, 1995), the REE (Cherniak, 2003a), Si (Cherniak, 2003b), Ba (Cherniak, 2002), and Mg (Van Orman et al., 2014).

Diffusion data for Ti in K-feldspar are plotted in Figure 3 and presented in Table 3. There is little evidence of diffusional anisotropy when comparing diffusivities normal to (010) and (001). Diffusivities are also similar for diffusion in air and under NNO-buffered conditions, as well as for the experiment conducted with glycine in the capsule, indicating little effect on Ti diffusion of fO_2 or the presence of hydrous species. For diffusion normal to (001), considering all data for this orientation, an activation energy of 342 ± 47 kJ mol^{-1} and a pre-exponential factor $3.01x10^{-6}$ m^2s^{-1} ($\log D_o = -5.52 \pm 2.06$) are obtained.

Time series at 900∝C were conducted for Ti diffusion normal to (001) in both oligoclase and K feldspar, with experiments run for times ranging from 17 hours to 141 hours for oligoclase, and one day to one week for K-feldspar (figure 4). In both cases, diffusivities agree within experimental uncertainty, suggesting that volume diffusion is the dominant contributor to the observed diffusion profiles.

There are clear differences in Ti diffusion for different feldspar compositions (Figure 7). Diffusion of Ti in K feldspar has a significantly higher activation energy for diffusion than in plagioclase. Over the temperature range of our experiments, Ti diffusion in K-feldspar is bracketed by diffusivities for oligoclase and labradorite. The greater activation energy for Ti diffusion in K feldspar results in significant differences in diffusivities at lower temperatures; for example, at 500°C, Ti diffusivities in K-feldspar and oligoclase would differ by two orders of magnitude.

In plagioclase, diffusivities differ with An content, with more calcic plagioclase having lower Ti diffusivities. Our data can be used to formulate an expression relating Ti diffusivity and An content of plagioclase. To obtain this estimate, we plot the diffusion coefficients at 900°C for oligoclase, labradorite, and albite, and extrapolate down-temperature to obtain a value for D at

that temperature for anorthite using an activation energy of 200 kJ/mol. The data approach a linear dependence of log D on An content (in mol%), and can be described by the expression -19.48 - (0.031*An) (Figure 5). This can be extended to a generalized expression with log D_o = (-10.49 - (0.031*An)) for an activation energy of 200 kJ/mol.

Comparison with diffusivities of other elements in Feldspar

Diffusion data for other cations in feldspar are plotted along with Ti in Figure 6. In oligoclase, Ti diffuses about two orders of magnitude faster than Si. Ti diffusion is also faster than Si diffusion in other plagioclase compositions, and has a lower activation energy for diffusion. Given the differences between Si and Ti diffusion, it may be that Ti preferentially migrates on tetrahedral sites occupied by Al, as the ionic radius of Ti^{+4} more closely matches Al (0.42 vs. 0.39 Å, for Ti and Al, respectively, Shannon, 1976).

Comparing to cations sited on M-sites, Ti diffuses faster than the trivalent REE. Because of the relatively low activation energy for diffusion in for Ti in oligoclase, Ti will diffuse faster than the large divalent cation Ba at low temperatures. Ti diffusion is more than 2 orders of magnitude slower than Sr and Pb diffusion (normal to (001)), and about 4 orders of magnitude slower than Mg diffusion. Univalent K also diffuses considerably faster (by about three orders of magnitude) than Ti. In labradorite, similar trends exist, but rates of Ti diffusion are closer to Si. Ti diffusion is considerably faster than CaAl-NaSi interdiffusion under dry conditions (Grove et al., 1984; Yund, 1986). While CaAl-NaSi interdiffusion may be enhanced by the presence of hydrous species (Yund, 1986; Yund and Snow, 1989; Liu and Yund, 1992) it is slower than Ti diffusion except at relatively high temperatures.

In K-feldspar, Ti diffuses about 2 orders of magnitude slower than Sr and Pb, 4 orders of magnitude slower than Rb, and 6 orders of magnitude slower than K. No data exist for Si or trivalent cations.

Our data indicate that Ti will be relatively resistant to diffusional alteration in all of the feldspar compositions. The implications of this will be discussed in later sections. It is important to note, however, that Ti concentrations in these experiments are relatively high in comparison to those often observed in natural plagioclase and K-feldspar, but diffusivities measured for specific feldspar compositions are in agreement for experiments using sources with differing Ti concentrations. Considering the detection limits for Ti in the analyses, and concentration ranges of Ti in diffusion experiments in the present study, the occurrence of differing diffusion mechanisms at lower concentrations of Ti cannot be precluded. Although the potential effects of concentration on Ti diffusion cannot be fully resolved by this study, we apply our diffusion data (with these caveats) in simple calculations examining retentivity of Ti chemical signatures, along with modeling of trace element redistribution accompanying feldspar exsolution, in the sections that follow.

Ti diffusion other mineral phases and retentivity of Ti chemical signatures

Figure 7 presents a summary of extant data for diffusion of Ti in minerals employed in crystallization geothermometers, along with Ti diffusion in feldspar. The mineral-element pairs involving Ti increasingly used in geothermometery are Ti in zircon (Watson and Harrison, 2005; Watson et al., 2006; Ferry and Watson, 2007) and Ti in quartz (Wark and Watson, 2006; Thomas et al., 2010). The measurement of Ti diffusivities for these minerals (Cherniak and Watson, 2007; Cherniak et al., 2007) can be used to evaluate the relative robustness of these

geothermometers when the relevant phases experience subsolidus thermal events following crystallization.

Diffusion of Ti in the feldspar is much faster than Ti diffusion in zircon, but slower than Ti diffusion in quartz. For example, at 900°C, Ti diffusion in oligoclase will be more than 10 orders of magnitude faster than Ti diffusion in zircon, and an order of magnitude slower than Ti diffusion in quartz. At this temperature, Ti diffusion in labradorite and orthoclase will be about 2 and 1.5 orders of magnitude slower, respectively, than Ti diffusion in quartz.

Also plotted are diffusion data for Ti in olivine and pyroxene from the studies of Cherniak and Liang (2012; 2014). Ti diffusion in feldspar is faster than Ti diffusion in olivine and pyroxene, with diffusivities higher by ~1-3 orders of magnitude, depending on feldspar composition.

The relative abilities of these mineral phases to preserve Ti concentrations that reflect conditions of crystallization can be illustrated with a few simple calculations of circumstances under which resetting of Ti signatures may occur. We consider a simple model in which the zircon, feldspar and quartz grains are spheres with radii a and initial uniform concentration of C_I, and are exposed to a medium with concentration C_o. The solution to the diffusion equation at the center of the spheres can then be derived (e.g., Crank, 1975) given these conditions. When the dimensionless parameter Dt/a^2 (where D is the diffusion coefficient and t is the time) is less than or equal to 0.03, the concentration at the center of the grain remains unchanged from its initial value. Above 0.03, the concentration at the center of the grain is affected by the externally imposed concentration C_o.

In Figure 8 we plot sets of curves for Dt/a^2 equal to the values of these dimensionless parameters, using effective diffusion radii differing with mineral type to reflect typical grain

sizes, using 0.5 mm for quartz and feldspar, and 50 μm for zircon. These curves define the time-temperature limits under which initial Ti compositional information will be retained in the grain centers of each of these phases. For times and temperatures below the curves, concentrations at crystal cores will remain unaffected, but will be influenced by the surrounding medium when conditions above the curves apply. These curves suggest that Ti chemical signatures may be preserved in feldspars under some geologic conditions. For example, this information will be preserved at 700°C in 0.5mm radius grains for ~5 Ma for oligoclase, ~70 Ma for labradorite, and ~170 Ma for K feldspar. In comparison, conditions for preservation of initial Ti concentrations in quartz grain centers at this temperature would be 1.5 Ma.

It should be emphasized that in these simple calculations and those that follow in this section assume that the feldspar grains are uniform in major-element composition, and that there are no processes such as exsolution occurring during heating or cooling trajectories that would result in compositional variations, and thus variations in Ti diffusivities.

The simple analysis above considers only isothermal conditions, so we can also explore the case of linear cooling from a given peak temperature. Watson and Cherniak (1997) noted that for linear cooling, a critical cooling rate that will preserve isotopic or chemical signatures in the center of a grain (the "center retention" criterion outlined above) will have a log-linear relationship with the inverse of the peak temperature. Their conclusion was based on numerical simulations of cooling paths, and an analytical expression has been developed that approximates this relationship (Watson and Cherniak, 2013; Cherniak and Watson, 2007):

$$\left(\frac{dT}{dt}\right)_c = \frac{RD_o T_{peak}^2}{E_a K a^2} \exp\left(\frac{-E_a}{RT_{peak}}\right) \quad (1)$$

where K is a constant (in these calculations, the same value as for the "center retention" criteria above will be used), R is the gas constant, a is the grain radius, E_a and D_o are the diffusion parameters (activation energy and pre-exponential factor), $(dT/dt)_c$ is the cooling rate, and T_{peak} is the peak temperature. In Figure 9, we plot critical cooling rates vs. peak temperature for K-feldspar, labradorite, and oligoclase of 500μm radii. For a peak temperature of 700°C, oligoclase of 500 μm radius would require cooling rates above ~ 8°C/Ma to maintain Ti signatures in their cores; labradorite and K feldspar would require cooling rates of above 1.5°C/Ma and 0.13°C/Ma, respectively, for a peak T of 700°C. For an 500°C peak temperature, Ti signatures in cores of feldspars would be retained even for very slow cooling, e.g., $7x10^{-3}$°C/Ma for oligoclase.

Preservation of Ti zoning

We can also consider conditions under which fine-scale chemical zoning in feldspar may be retained or lost. For these estimates, we use a simple model, with zones modeled as plane sheets of thickness l; adjacent planes have different concentrations of diffusant. Only diffusion normal to the planar interface is considered. A (somewhat arbitrary) criterion for alteration of zones is employed. Zones are considered to be "lost" if a compositional change of 10% is attained in the zone's center. When this condition applies, the dimensionless parameter Dt/l^2 will be equal to $3.3x10^{-2}$. Figure 10 shows curves constraining the time-temperature conditions under which Ti zoning of 10 and 100μm width will be retained in labradorite, oligoclase and K-feldspar given the above criteria. In oligoclase, for example, 100μm scale zones would resist being obliterated at 700°C for about 200,000 years, with 10μm zones being preserved for up to 2,000 years. In labradorite, these times would be 1 million years and 10,000 years for 100μm and 10μm zones, respectively. More sodic plagioclase would lose Ti zoning more rapidly, and more calcic

plagioclase more slowly; for example, at 700°C, 100μm zones would be lost in albite in ~20,000 years, and ~10 million years in anorthite. For the case of K-feldspar, 10 and 100μm zones would be preserved at 700°C for up to ~80,000 and 8 million years, respectively.

We can also use this approach to consider the relative retentivity of Ti zoning compared with that of other trace and minor elements in feldspar. In oligoclase, for example (Figure 11) 50μm zones would be preserved at 600°C for durations of ~ 1 million years. Both Sr and Mg zoning would be lost at this temperature over much shorter timescales -- about 70,000 years and 3,000 years for Sr and Mg, respectively. In contrast, Ba zoning would be better preserved, with 50μm zones preserved for times up to 20 million years at 600°C. Given the relative differences in cation diffusivities in labradorite, there would be a similar pattern in relative retentivity of zoning. It is clear from these simple calculations that Ti (as well as Ba) compositional zoning in feldspars may be among the more robust geochemical indicators of magma evolution.

Trace element redistribution accompanying exsolution in alkali feldspars

Armed with a new diffusion law for a trace species (Ti^{4+}) that diffuses more slowly than most other impurities in alkali feldspar, it may be instructive to examine the redistribution of trace elements that accompanies exsolution of sodic feldspar from a K-rich feldspar host. A similar phenomenon has been explored in models of element redistribution during formation of the Widmanstätten pattern in iron meteorites, which develops when lamellae of Ni-poor kamacite exsolve from originally homogeneous taenite. Goldstein and co-workers pioneered the modeling of Fe-Ni redistribution during cooling of iron meteorites (e.g., Moren and Goldstein 1979), and Watson and Watson (2003) extended the strategy to a variety of siderophile trace elements in the same system. Just as the Fe-Ni system has constrained cooling rates of meteorite parent bodies, the combined kinetics of feldspar lamellar growth and trace-element diffusion have the potential

353 to shed light on thermal histories of host rocks. Here we demonstrate this potential by
354 characterizing elemental profiles across an albite lamella in K-feldspar and attempting to
355 reproduce selected profiles in numerical models based on assumed t-T histories and lamellar
356 growth rates.

357 The first step was to measure profiles of major elements and selected trace elements (Ti, Sr,
358 Ba, Rb) across the boundary between an exsolved albite lamella and host K-feldspar from a
359 pegmatite vein in Colorado (EchoHawk and Kackstaetter 2016) using laser-ablation ICP/MS
360 with a 193-nm excimer laser. This is not an ideal instrument for the purpose because of
361 inevitable analytical spreading caused by the laser footprint and wash-out time, but it was the
362 only analytical method available to us that enabled characterization of the full profiles of all the
363 elements of interest (the concentrations of most trace elements in the albite lamella are <5 ppm).
364 To obtain the necessary sensitivity, the sample was translated at 1 μm/s under a ~180×10-micron
365 laser spot (rep rate = 10 Hz) with the long dimension parallel to the albite/K-feldspar interface.
366 Assuming the interface to be infinitely sharp with respect to Na and K (Figure 12a), the
367 analytical spreading at these conditions along a traverse across this boundary is 20-30 μm, as can
368 be seen in the Na profile in Figure 12b. The shapes of all analytical profiles must therefore be
369 assumed to be rounded and damped to some extent, but we believe they are adequate for a
370 preliminary proof-of-concept study. Elemental profiles for Na, Sr, Rb, Ba and Ti are shown in
371 Figures 12b-12f, respectively.

372 Attempts were made to reproduce some of the measured profiles using a moving boundary
373 finite-difference computer program similar to those described by Watson and Watson (2003) and
374 Watson and Müller (2009); details of the methods can be found in those papers. In a broad
375 sense, these programs capture the redistribution of trace elements, governed by diffusion and

local partitioning equilibrium at the two-feldspar interface, as one phase grows at the expense of another. In the natural system, coarsening of the lamella is controlled by the rate of Na-K interdiffusion, which is faster than all trace elements considered here (Yund and Davidson 1978). In general, coarsening is expected to depend on the cube root of time (Owen and McConnell, 1974; Yund and Davidson 1978), but because the appropriate rate law for geological coarsening is not known, we resorted for simplicity to exploring constant coarsening rates that seemed geologically plausible given the ~60-micron width of the analyzed lamella (Figure 12a). Growth rates were calculated by assuming geological "annealing" durations of 60, 6 and 0.6 MYr to produce the observed lamellar half-width of ~30 microns at assumed temperatures of 550°, 600° and 650°C. The ranking (fastest to slowest) of the diffusivities of the measured elements is Rb > Sr > Ba > Ti at assumed temperatures of 600±50°C, as can be deduced from Figure 5. To our knowledge, Ba diffusion has not been characterized in K-feldspar specifically, but this element diffuses more slowly than Sr in other feldspars where it has been measured (e.g., Cherniak, 2010). Most of the trace elements investigated here are partitioned strongly into K-feldspar relative to albite, so migration of the albite/K-feldspar interface (i.e., growth of albite at the expense of K-feldspar) produces a "snowplow" or pileup effect on elemental concentration in the K-feldspar near the moving interface. This effect is particularly evident in the cases of Sr and Ba (Figures 12c and 12e), where pronounced concentration spikes are present in the K-feldspar on either side of the albite lamella [the right-hand side is less well developed due to the irregular interface (see Figure 12a), so we focus here on the left side]. We attempted to reproduce the spikes by running numerical simulations specifically for Sr because diffusion laws for both K-feldspar and albite are available for this element (see Cherniak 2010), and because the Sr pileup feature is clearly evident. The albite/K-feldspar partition coefficient was estimated from the

399 laser traverse to be roughly 0.17 based on the ratio of the relatively flat concentration profile in
400 the albite to the maximum of the Sr spike in the adjacent K-feldspar. The rationale for this
401 choice is that equilibrium is maintained at the albite/K-feldspar interface. This approximate
402 partition coefficient was an input parameter for the numerical models.. The model results are
403 overlain as bold lines on the left side of the Sr profile in Figure 12c, revealing a similarity in
404 height and width of the model profiles and the actual one. Despite wide variation in the assumed
405 growth rates and durations (see inset on the figure), the three computed profiles are nearly the
406 same, which illustrates the non-uniqueness of forward models of this sort for a single element, as
407 well as the compensating effects of growth rate and duration (the product of the growth rate and
408 duration is the same for the three model outcomes shown, indicating that for Sr the magnitude of
409 the snowplow effect depends mainly on the extent of lamellar growth). It is important to note
410 that the concentrations of Sr, Rb and Ba across the albite lamella appear to be relatively flat.
411 This is because diffusion in albite (relative to K-feldspar) is fast, and also because these elements
412 are strongly partitioned into the K-feldspar at the interface during growth—so the concentrations
413 in the albite are very low. A slight climb in concentration approaching the K-feldspar would be
414 expected, but this tends to be leveled by diffusion and cannot be resolved anyway because of the
415 limited spatial resolution of the laser analyses.
416 Quantitative models for Rb, Ba and Ti are more difficult to produce due to the lack of
417 appropriate diffusion laws and/or indistinct features in the profiles. Some generalizations are
418 nevertheless possible. In the case of Rb, for example, relatively fast diffusion in K-feldspar
419 appears to have suppressed development of concentration spikes (pileup) near the interface
420 despite rejection of Rb from the growing albite—i.e., Rb concentration anomalies seem to have
421 been flattened by diffusion. Barium, whose diffusivity in K-feldspar is probably lower than that

of Sr, shows a somewhat narrower and higher concentration spike than Sr, as expected. The key element targeted for diffusion measurements in this study (Ti) was also the most challenging to analyze in the feldspar because of its low concentration. However, the general character of the profile seems clear: no flat bottom in the albite and no concentration spikes in the K-feldspar. At first glance, the absence of spikes seems to mimic the profile for fast-diffusing Rb, but in fact the spikes might be missing for a different reason. Given the slow diffusion of Ti relative to the other elements examined (especially Rb), the "snowplow" effect would be expected to produce an extremely sharp concentration spike due to the near-absence of diffusive spreading into the K-feldspar. Such a feature might well be too narrow to detect because of the limited spatial resolution of the laser. Alternatively, lamellar growth might be fast enough to "overrun" the expected redistribution of Ti by diffusion, as observed by Koga et al. (1999) in the case of rare-earth element behavior during the conversion of clinopyroxene to orthopyroxene in decompressing peridotite transitioning from the garnet to the spinel facies. Indeed, attempted numerical simulations suggest that the growth rates needed for the models to capture the general character of the Sr spikes (Figure 12c) are sufficiently fast compared with Ti diffusion that the interface sweeps through the feldspar structure with no opportunity for Ti to diffuse away or to establish local partitioning equilibrium at the interface between the two feldspars. This implies that under some circumstances—a fast-moving interface combined with slow impurity diffusion—a phase boundary might advance through a material with minimal redistribution of impurities. The dip in Ti content in the albite is probably a consequence of partial Ti redistribution during albite growth. In a limited sense, our failure to produce a convincing result for the element targeted in this diffusion study is disappointing, but the apparent success with Sr suggests that the general approach might be successful for Ti and other elements in other

samples. If coarsening rates of feldspar lamellae (controlled by Na↔K interdiffusion) can be better constrained for geological timescales, it may be possible to pursue strategies like those developed by Goldstein and co-workers for estimating cooling rates of iron meteorite parent bodies (see Moren and Goldstein 1979).

Due to limitations in the measured profiles and available diffusion laws, the model results in this section have provided no quantitative insight into thermal histories, nor have they definitively characterized Ti behavior during alkali feldspar exsolution. We hope, however, that the potential of the general approach has come through, and that the advantages of having available a variety of diffusion laws are evident. Improved spatial resolution of Ti analyses (without loss of analytical sensitivity) may reveal features in Ti profiles across exsolution boundaries that were not detectable in this study by LA-ICP/MS. The addition of new data for a trace impurity (Ti) that is slow-diffusing and ubiquitous in feldspars (Hoff and Watson 2018) should expand the scope and applicability of *t-T* models for crustal rocks based on trace elements in feldspars.

Implications

These data indicate that feldspar should be moderately retentive of Ti chemical signatures, depending on feldspar composition. Ti diffuses more slowly than most other impurities in feldspar, including Sr. In the case of plagioclase, a dependence of Ti on feldspar An content is evident, with an increase of 30% in An content resulting in a decrease in diffusivity of about an order of magnitude.

This characterization of diffusivities for a trace impurity that is relatively slow-diffusing and ubiquitous in feldspars (Hoff and Watson, 2018) has the potential to expand the scope and applicability of modeling of time-temperature conditions for crustal rocks based on trace

elements in feldspars. These data could be applied, for example, in examining the redistribution of trace elements that accompany exsolution of sodic feldspar from a K-rich feldspar host, by modeling profiles obtained from major and trace element traverses across lamellar boundaries.

Acknowledgements – Thanks to Christopher Hoff for providing the feldspar sample with exsolved albite lamella and to him and Jared Singer for performing the LA-ICP/MS traverses on the sample. We thank two anonymous reviewers for their constructive comments. This work was supported by NSF grant no. 1551381 to EBW.

References

Adams, D.T., Nielsen, R.L., Kent, A.J.R., and Tepley III, F.J. (2011) Origin of minor and trace element compositional diversity in anorthitic feldspar phenocrysts and melt inclusions from the Juan de Fuca Ridge. G-cubed 12, 12. doi:10.1029/2011GC003778

Ageeva, O., Habler, G., Topa, D., Waitz, T., Li, C., Pertsev, A., Griffiths, T., Zhilicheva, O., and Abart, R. (2016) Plagioclase hosted Fe-Ti oxide micro-inclusions in an oceanic gabbro plagiogranite association from the Mid-Altlantic Ridge at 13°34' N. American Journal of Science 316, 85-109.

Behrens, H., Johannes, W., and Schmalzried, H. (1990) On the mechanisms of cation diffusion processes in ternary feldspars. Physics and Chemistry of Minerals 17, 62-78.

Beyer, C., Dohmen, R., Rogalla, D., Becker, H.-W., Marquardt, K., Vollmer, C., Hagemann, U., Hartmann, N., and Chakraborty, S. (2019) Lead diffusion in $CaTiO_3$: A combined study using Rutherford backscattering and TOF-SIMS for depth profiling to reveal the role of lattice strain in diffusion processes. American Mineralogist 104, 557-568.

Cherniak, D.J. (1995) Diffusion of Pb in plagioclase and K-feldspar measured by Rutherford Backscattering spectroscopy and resonant nuclear reaction analysis. Contributions to Mineralogy and Petrology 120, 358-371.

Cherniak, D.J. (1996) Strontium diffusion in sanidine and albite, and general comments on Sr diffusion in alkali feldspars. Geochimica et Cosmochimica Acta 60, 5037-5043.

Cherniak, D.J. (2002) Ba diffusion in feldspar. Geochimica et Cosmochimica Acta 66, 1641-1650.

Cherniak, D.J. (2003a) REE diffusion in feldspar. Chemical Geology 193, 25-41.

Cherniak, D.J. (2003b) Silicon self-diffusion in single-crystal natural quartz and feldspar. Earth and Planetary Science Letters 214, 655-668.

Cherniak, D.J. (2010) Cation diffusion in feldspars. In Y. Zhang and D. Cherniak, Eds., Diffusion in Minerals and Melts, 41, p. 691-733Reviews in Mineralogy and Geochemistry, Mineralogical Society of America, Chantilly, Virginia.

Cherniak, D.J. (2008) Si diffusion in zircon. Physics and Chemistry of Minerals 35, 179-187.

Cherniak, D.J., and Liang, Y. (2014) Titanium diffusion in olivine. Geochimica et Cosmochimica Acta 147, 43-57.

Cherniak, D.J., and Liang, Y. (2012) Ti diffusion in natural pyroxene. Geochimica et Cosmochimica Acta 98, 31-47.

Cherniak, D.J., and Watson, E.B. (2007) Ti diffusion in zircon. Chemical Geology 242, 473-486.

Cherniak, D.J., and Watson, E.B. (2001) Pb Diffusion in zircon. Chemical Geology 172, 5-24.

Cherniak, D.J., and Watson, E.B. (1994) A study of strontium diffusion in plagioclase using Rutherford Backscattering Spectroscopy. Geochimica et Cosmochimica Acta 58, 5179-5190.

518 Cherniak, D.J., and Watson, E.B. (1992) A study of strontium diffusion in K-feldspar, Na-K
519 feldspar and anorthite using Rutherford Backscattering Spectroscopy. Earth and Planetary
520 Science Letters 113.
521 Cherniak, D.J., Watson, E.B., and Wark, D.A. (2007) Ti diffusion in quartz. Chemical Geology
522 236, 65-74.
523 Cherniak, D.J., Watson, E.B., Grove, M., and Harrison, T.M (2004) Pb diffusion in monazite: a
524 combined RBS/SIMS study. Geochimica et Cosmochimica Acta 68, 829-840.
525 Cherniak, D.J., Hanchar, J.M., and Watson, E.B. (1997) Rare earth diffusion in zircon. Chemical
526 Geology 134, 289-301.
527 Crank, J. (1975) The Mathematics of Diffusion (2nd ed.), Oxford, 414 pp.
528 Dohmen, R., Marschall, H.R., Ludwig, T., and Polednia, J. (2019) Diffusion of Zr, Hf, Nb and
529 Ta in rutile: effects of temperature, oxygen fugacity, and doping level, and relation to rutile
530 point defect chemistry Physics and Chemistry of Minerals 46, 311–332
531 EchoHawk, B., and Kackstaetter, U. (2016) Roadside faults, folds, fossils, crystals, and diamond
532 pipes—sampling the geologic diversity of northern Colorado. Geological Society of America
533 Field Guide 44, stop 3.
534 Ferry, J.M., and Watson, E.B. (2007) New thermodynamic models and revised calibrations for
535 the Ti-in-zircon and Zr-in-rutile thermometers. Contributions to Mineralogy and Petrology
536 154, 429-437.
537 Foland, K.A. (1974) Alkali diffusion in orthoclase. In A.W. Hofmann, B.J. Giletti, H.S. Yoder,
538 Jr., and R.A. Yund, Eds., Geochemical Transport and Kinetics. Carnegie Institution of
539 Washington Publication, 634, p. 77-98. Carnegie Institution of Washington, Washington,
540 DC.

Giletti, B. J. (1991) Rb and Sr diffusion in alkali feldspars, with implications for cooling histories of rocks. Geochimica et Cosmochimica Acta 55, 1331-1343.

Giletti, B. J., and Casserly, J.E.D. (1994) Sr diffusion kinetics in plagioclase feldspars. Geochimica et Cosmochimica Acta 58, 3785-3793.

Giletti, B.J., and Shanahan, T.M. (1997) Alkali diffusion in plagioclase feldspar. Chemical Geology 139, 3-20.

Ginibre, C., Wörner, G., and Kronz, A. (2004) Structure and dynamics of the Laacher see magma chamber (Eifel, Germany) from major and trace element zoning in sanidine: A cathodoluminescence and electron microprobe study. Journal of Petrology, 45, 2197–2223.

Grove, T.L., Baker, M.B., and Kinzler, R.J. (1984) Coupled CaAl-NaSi diffusion in plagioclase feldspar: experiments and applications to cooling rate speedometry. Geochimica et Cosmochimica Acta 48, 2113-2121.

Hergemöller, F., Wegner, M., Deicher, M., Wolf, H., Brenner, F., Hutter, H., Abart, R., and N.A., Stolwijk (2017) Potassium self‐diffusion in a K‐rich single‐crystal alkali feldspar. Physics and Chemistry of Minerals 44, 345–351.

Hoff, C. (2019) Defect thermometry using rutile and feldspar, 103p. Ph.D. thesis, Rensselaer Polytechnic Institute.

Hoff, C., and Watson, E.B. (2018) TITANOR: A Titanium-in-potassium feldspar thermometer. Geological Society of America Annual Meeting (abstract), paper 137-7.

Jeynes, C. and Colaux, J.L. (2016) Thin film depth profiling by ion beam analysis. Analyst 141, 5944-5985.

Kasper, R. B. (1975) Cation and oxygen diffusion in albite, 156 p. Ph.D. thesis, Brown University.

564 Koga, K.T., Shimizu, N. and Grove, T.L. (1999) Disequilibrium trace element re-distribution
565 during garnet to spinel facies transformation. In Proc. 7th Intl. Kimberlite Conf. J. J. Gurney
566 et al., eds. , Red Roof design, Cape Town, p. 444 - 451.
567 LaTourette, T., and Wasserburg, G.J. (1998) Mg diffusion in anorthite: implications for the
568 formation of early solar system planetisimals. Earth and Planetary Science Letters 158, 91-
569 108.
570 Liu, M., and Yund, R.A. (1992) NaSi-CaAl interdiffusion in plagioclase. American Mineralogist
571 77, 275-283.
572 Moren, A.E., and Goldstein, J.I. (1979) Cooling rates of group-Iva iron-meteorites determined
573 from a ternary Fe-Ni-P model. Earth and Planetary Science Letters 43, 182-196.
574 Norberg, N., Harlov, D., Neusser, G., Wirth, R., and Rheden, D. (2014) Element mobilization
575 during feldspar metasomatism: an experimental study. European Journal of Mineralogy 26,
576 71–82.
577 Owen, D.C., and McConnell, J.D.C. (1974) Spinodal unmixing in an alkali feldspar. In W.S.
578 MacKenzie and J. Zussman, Eds., The Feldspars, p. 424-439, Manchester University Press.
579 Parsons, I., Steele, D.A., Lee, M.R., and Magee, C.W. (2008) Titanium as a
580 cathodoluminescence activator in alkali feldspars. American Mineralogist 93, 875-879.
581 Peters, M.T., Shaffer, E.E., Burnett, D.S., and Kim, S.S. (1995) Magnesium and titanium
582 partitioning between anorthite and Type B CAI liquid: Dependence on oxygen fugacity and
583 liquid composition. Geochimica et Cosmochimica Acta 59, 2785-2796.
584 Salmonsen, L., Tegner, C., and Humphreys, M. (2011) Titanium in plagioclase as a monitor of
585 magma differentiation in the Skaergaard Intrusion. Abstract, AGU Fall Meeting

586 Schaffer, A.-K., Petrishcheva, E., Habler, G., Abart, R., Rhede, D., and Giester, G. (2014)
587 Sodium-potassium interdiffusion in potassium-rich alkali feldspar II: Composition and
588 temperature dependence obtained from cation exchange experiments.. American Journal of
589 Science, 314, 1300–1318.
590 Singer, B.S., Dungan, M.A., and Layne, G.D. (1995) Textures and Sr, Ba, Mg, Fe, K, and Ti
591 compositional profiles in volcanic plagioclase: Clues to the dynamics of calc-alkaline magma
592 chambers. American Mineralogist 80, 776-798.
593 Shannon, R.D. (1976) Revised effective ionic radii and systematic studies of interatomic
594 distances in halides and chalcogenides. Acta Crystallographica A32, 751-767.
595 Thomas, J.B., Watson, E.B., Spear. F.S., Shemella, P.T., Nayak, S.K., and Lanzirotti, A. (2010)
596 TitaniQ under pressure: the effect of pressure and temperature on the solubility of Ti in
597 quartz. Contributions to Mineralogy and Petrology 160,743–759.
598 Van Orman, J.A. Cherniak, D.J., and Kita, K.T. (2014) Magnesium diffusion in plagioclase:
599 Implications for thermal resetting of the ^{26}Al-^{26}Mg early solar system chronometer. Earth and
600 Planetary Science Letters 385, 79-88.
601 Wark, D.A., and Watson, E.B. (2006) TitaniQ: A Titanium-in-Quartz Geothermometer.
602 Contributions to Mineralogy and Petrology 152, 743-754.
603 Watson, E.B., and Cherniak, D.J. (1997) Oxygen diffusion in zircon. Earth and Planetary
604 Science Letters 148, 527-544.
605 Watson, E.B., and Cherniak, D.J. (2013) Simple equations for diffusion in response to heating.
606 Chemical Geology 335, 93-104.
607 Watson, E.B., and Harrison, T.M. (2005) Zircon thermometer reveals minimum melting
608 conditions on earliest Earth, Science 308, 841-844.

609 Watson, E.B., and Müller, T. (2009) Non-equilibrium isotopic and elemental fractionation during
610 diffusion-controlled crystal growth under static and dynamic conditions. Chemical Geology
611 267, 111-124.
612 Watson, E.B., Wark, D.A., and Thomas, J.B. (2006) Crystallization thermometers for zircon and
613 rutile, Contributions to Mineralogy and Petrology 151,413-433.
614 Watson, H.C., and Watson, E.B. (2003) Siderophile trace element diffusion in Fe-Ni alloys.
615 Physics of the Earth and Planetary Interiors 139, 65-75.
616 Wenk, H.-R., Chen, K., and Smith, R. (2011) Morphology and microstructure of magnetite and
617 ilmenite inclusions in plagioclase from Adirondack anorthositic gneiss. American
618 Mineralogist 96, 1316-1324.
619 Wilangowski, F., Abart, R., Divinski, S.V., and Stolwijk, N.A. (2015) Radiotracer experiments
620 and Monte Carlo simulations of sodium diffusion in alkali feldspar: Evidence against the
621 vacancy mechanism. Defect and Diffusion Forum 363,79-84.
622 Yund, R.A. (1986) Interdiffusion of NaSi-CaAl in peristerite. Physics and Chemistry of Minerals
623 13, 11-16.
624 Yund, R.A., and Davidson, P. (1978) Kinetics of lamellar coarsening in cryptoperthites.
625 American Mineralogist 63, 470-477.
626 Yund, R.A., and Snow, E. (1989) Effects of hydrogen fugacity and confining pressure on the
627 interdiffusion rate of NaSi-CaAl in plagioclase. Journal of Geophysical Research B 94,
628 10,662-10,668.
629

This is a preprint, the final version is subject to change, of the American Mineralogist (MSA)
Cite as Authors (Year) Title. American Mineralogist, in press.
DOI: https://doi.org/10.2138/am-2020-7272

630 **Table 1. Compositional information for feldspars**
631 **used in this study**. *(wt% oxides)*

	K Feldspar	Albite	Oligoclase	Labradorite	Anorthite
SiO_2	65.44	68.28	62.73	51.45	45.13
Al_2O_3	17.66	19.23	22.89	29.59	35.46
FeO	0.75	0.01	0.05	0.40	0.54
CaO	0.01	0.03	4.48	13.62	18.85
K_2O	15.41	0.22	0.64	0.15	0.03
Na_2O	0.75	11.63	8.81	3.80	0.71
total	100.02	99.40	99.60	99.01	100.72

632
633

This is a preprint, the final version is subject to change, of the American Mineralogist (MSA)
Cite as Authors (Year) Title. American Mineralogist, in press.
DOI: https://doi.org/10.2138/am-2020-7272

Table 2. Ti Diffusion in Plagioclase

	T(°C)	*time(sec)*	*D(m^2sec^{-1})*	*log D*	*+/-*	*source†*	*buffer*
Oligoclase (An_{23})							
diffusion normal to (001):							
TiOlig-9	752	$8.50x10^5$	$1.74x10^{-22}$	-21.76	0.36	TiO_2	air
TiOlig-7	800	$2.48x10^5$	$8.51x10^{-22}$	-21.07	0.37	TiAl-3	air
TiOlig-11	800	$8.08x10^5$	$6.17x10^{-22}$	-21.21	0.43	TiAl-3	air
TiOlig-6	850	$5.04x10^5$	$2.24x10^{-21}$	-20.65	0.30	TiAl-3	air
TiOlig-20	850	$5.18x10^5$	$1.36x10^{-21}$	-20.87	0.46	TiAl-10	NNO
TiOlig-8	900	$6.12x10^4$	$4.72x10^{-21}$	-20.33	0.38	TiO_2	air
TiOlig-16	900	$1.92x10^5$	$2.16x10^{-21}$	-20.66	0.30	TiAl-10	air
TiOlig-17	900	$5.08x10^5$	$2.98x10^{-21}$	-20.53	0.32	TiAl-10	air
TiOlig-14	950	$1.44x10^4$	$2.56x10^{-20}$	-19.59	0.45	TiO_2	air
TiOlig-18c	950	$2.48x10^5$	$8.20x10^{-21}$	-20.09	0.23	TiAl-10	air
TiOlig-19	950	$2.43x10^5$	$8.34x10^{-21}$	-20.08	0.28	TiAl-10	NNO
TiOlig-12	1000	$3.60x10^3$	$3.35x10^{-20}$	-19.48	0.45	TiO_2	air
TiOlig-22	1003	$2.88x10^4$	$1.39x10^{-20}$	-19.86	0.38	TiAl-10	NNO
TiOlig-13	1050	$1.80x10^3$	$1.05x10^{-19}$	-18.98	0.44	TiO_2	air
diffusion normal to (010):							
TiOlig-21	851	$6.05x10^5$	$1.50x10^{-21}$	-20.82	0.45	TiAl-10	air
TiOlig-18b	950	$2.48x10^5$	$5.60x10^{-21}$	-20.25	0.29	TiAl-10	air
TiOlig-23	1003	$2.16x10^4$	$2.40x10^{-20}$	-19.62	0.48	TiAl-10	air
Labradorite (An_{67})							
diffusion normal to (001):							
TiLab-4	900	$1.21x10^6$	$3.64x10^{-22}$	-21.44	0.35	TiAl-10	air
TiLab-2	950	$6.95x10^5$	$9.15x10^{-22}$	-21.04	0.42	TiAl-10	air
TiLab-5	999	$4.32x10^5$	$9.25x10^{-22}$	-21.03	0.44	TiAl-10	air
TiLab-1	1050	$2.48x10^5$	$3.93x10^{-21}$	-20.41	0.30	TiAl-10	air
TiLab-3	1150	$1.01x10^5$	$8.92x10^{-21}$	-20.05	0.33	TiAl-10	air
Anorthite (An_{93})							
diffusion normal to (010):							
TiAnorth-1	1050	$5.90x10^5$	$5.23x10^{-22}$	-21.28	0.41	TiAl-10	air
Albite (An_1)							
diffusion normal to (001):							
TiAlb-1	900	$8.64x10^4$	$4.33x10^{-20}$	-19.36	0.27	TiAl-10	air

† *TiAl-10: TiO_2-Al_2O_3 (10:1), TiAl-3: TiO_2-Al_2O_3 (3:1)*

This is a preprint, the final version is subject to change, of the American Mineralogist (MSA)
Cite as Authors (Year) Title. American Mineralogist, in press.
DOI: https://doi.org/10.2138/am-2020-7272

647 Table 3. Ti Diffusion in K-Feldspar

	T(°C)	*time(sec)*	*D(m^2sec^{-1})*	*log D*	*+/-*	*source†*	*buffer*
648 *diffusion normal to (001):*							
TiMO-9	799	$1.92x10^6$	$1.13x10^{-22}$	-21.95	0.43	TiAl-10	air
TiMO-4	852	$5.90x10^5$	$3.98x10^{-22}$	-21.40	0.37	TiO_2	air
TiMO-14	851	$6.01x10^5$	$9.23x10^{-22}$	-21.03	0.37	TiAl-10	NNO
TiMO-3	900	$1.62x10^5$	$2.54x10^{-21}$	-20.60	0.33	TiO_2	air
TiMO-6	900	$8.64x10^4$	$8.83x10^{-22}$	-21.05	0.48	TiAl-10	air
TiMO-7	900	$6.05x10^5$	$7.72x10^{-22}$	-21.11	0.29	TiAl-10	air
TiMO-1	950	$2.45x10^5$	$1.12x10^{-20}$	-19.95	0.24	TiO_2	air
TiMO-10c	950	$2.48x10^5$	$3.84x10^{-21}$	-20.42	0.45	TiAl-10	air
TiMO-12	950	$1.69x10^5$	$3.71x10^{-21}$	-20.43	0.24	TiAl-10	NNO
TiMO-13	950	$2.72x10^5$	$3.18x10^{-21}$	-20.50	0.44	TiAl-10	NNO- glycine
TiMO-5	1000	$5.76x10^4$	$7.15x10^{-20}$	-19.15	0.27	TiO_2	air
TiMO-16	1003	$2.88x10^4$	$3.50x10^{-20}$	-19.45	0.42	TiAl-10	NNO
649 *diffusion normal to (010):*							
TiMO-15	851	$6.05x10^5$	$1.13x10^{-21}$	-20.95	0.41	TiAl-10	air
TiMO-10b	950	$2.48x10^5$	$4.13x10^{-21}$	-20.38	0.28	TiAl-10	air
TiMO-17	1003	$2.16x10^4$	$4.73x10^{-20}$	-19.33	0.36	TiAl-10	air

650 † *TiAl-10: TiO_2-Al_2O_3 (10:1)*
651
652

653

654 **Captions for figures**

655 Figure 1. Typical Ti diffusion profiles for oligoclase (a, b) and K-feldspar (c, d) for experiments
656 run at 950ºC for 69 hours and 68 hours, respectively. In (a) and (c), the measured diffusion
657 profiles are plotted with complementary error function curves. In (b) and (d), the data are
658 linearized by inversion through the error function. Slopes of the lines are equal to $(4Dt)^{-1/2}$.

659

660 Figure 2. Arrhenius plot of Ti diffusion in plagioclase. For diffusion normal to (001) in
661 oligoclase, we obtain an activation energy of 207 ± 31 kJ/mol. and pre-exponential factor of
662 6.67×10^{-12} m^2/s ($\log D_o = -11.18 \pm 1.41$). There appears to be little dependence of Ti diffusion on
663 orientation, when comparing data for diffusion normal to (010) and (001) (black and white
664 circles, respectively), or fO_2, comparing experiments run in air and those under NNO-buffered
665 conditions (grey diamonds). In labradorite (dark grey squares), we obtain an activation energy of
666 181 ± 57 kJ/mol. and pre-exponential factor of 4.37×10^{-14} m^2/s ($\log D_o = -13.36 \pm 2.32$) for
667 diffusion normal to (001). Data for anorthite (white triangle) and albite (black triangle) indicate
668 a clear trend of decreasing diffusivities in more calcic plagioclase.

669

670 Figure 3. Arrhenius plot for Ti diffusion in K-feldspar. For diffusion normal to (001), an
671 activation energy of 342 ± 47 kJ mol^{-1} and a pre-exponential factor 3.01×10^{-6} m^2s^{-1} ($\log D_o = -$
672 5.52 ± 2.06) are obtained. There is little evidence of diffusional anisotropy when comparing
673 diffusivities normal to (010) and (001) (black and white circles, respectively). Diffusivities are
674 also similar for diffusion in air and under NNO-buffered conditions (grey triangles), as well as
675 for the experiment conducted with glycine in the capsule (dark grey square), indicating little
676 effect on Ti diffusion of fO_2 or the presence of hydrous species.

677

678 Figure 4. Time series at 900°C for oligoclase (a) and K feldspar (b). In both cases, diffusivities
679 agree within experimental uncertainty over a range of experiment durations, suggesting that
680 volume diffusion is the dominant contributor to the observed diffusion profiles.

681

682 Figure 5. Relationship between Ti diffusivity and An content of plagioclase. Diffusion
683 coefficients at 900°C for oligoclase, labradorite, and albite are plotted as a function of An
684 content, along with a down-temperature extrapolation for anorthite to obtain a value for D at that
685 temperature, using an activation energy of 200 kJ/mol. The data approach a linear dependence of
686 log D on An content (in mol%), and can be described by the expression -19.48 - (0.031*An).

687

688 Figure 6. Diffusion data for Ti and other cations in albite (a), oligoclase (b), labradorite (c),
689 anorthite (d) and K-feldspar (e). Sources for data: Ti - this study; Sr - Cherniak and Watson,
690 1992; 1994; Cherniak, 1996; Giletti and Casserly, 1994; Pb - Cherniak, 1995; Ba - Cherniak,
691 2002; REE- Cherniak, 2003a; Si - Cherniak, 2003b; Li - Giletti and Shanahan, 1997; Fe -
692 Behrens et al., 1990; Mg - plagioclase - Van Orman et al., 2014; Ca, Mg - anorthite - La Tourette
693 and Wasserburg, 1998; Ca - labradorite - Behrens et al., 1990; Rb - albite - Giletti and Shanahan,
694 1997; Rb - K feldspar - Giletti, 1991; K - K feldspar - Foland, 1974; Hergemöller et al., 2017; K
695 - plagioclase - Giletti and Shanahan, 1997; Na - K feldspar - Wilangowski et al., 2015; Foland,
696 1974; Na- albite - Kasper, 1975; Na - labradorite - Behrens et al., 1990.

697

698 Figure 7. Ti diffusion in feldspar and other minerals. Sources for data: feldspar - this study;
699 zircon- Cherniak and Watson, 2007; quartz - Cherniak et al., 2007; olivine- Cherniak and Liang,
700 2014; pyroxene - Cherniak and Liang, 2012.

Figure 8. Curves representing time-temperature conditions under which Ti signatures at the center of grains will be lost. For times and temperatures below the curves, concentrations at crystal cores will remain unaffected, but will be influenced by the surrounding medium when conditions above the curves apply. In calculations, diffusivities from the Arrhenius relations plotted in Figure 7 are used, and effective diffusion radii differing with mineral type are selected, using 0.5 mm for quartz and feldspar, and 50 μm for zircon. These curves suggest that feldspars may be relatively retentive of Ti chemical signatures under some geologic conditions. For example, this information would be preserved at 700°C in 0.5mm radius grains over timescales of ~5 Ma for oligoclase, ~70 Ma for labradorite, and ~170 Ma for K feldspar. In comparison, conditions for preservation of initial Ti concentrations in quartz grain centers at this temperature would be 1.5 Ma.

Figure 9. Ti center-retention criteria for feldspars of 500 μm radii cooling at a linear rate from a range of maximum temperatures T_{peak}. The critical cooling rate $(dT/dt)_c$, will depend on the maximum temperature, grain radius and diffusion parameters. When cooling rates are slower than this critical value, the peak-temperature Ti signature in the center of a feldspar grain will not be preserved over the cooling path. The lines are calculated using eq. 1.

Figure 10. Conditions for preservation of fine-scale chemical zoning of Ti in feldspar may be retained or lost. Zones are considered to be "lost" if a compositional change of 10% is attained in the zone's center. The curves constrain the time-temperature conditions under Ti zoning of 10

723 and 100μm width will be retained in labradorite, oligoclase and K-feldspar; for conditions below
724 the curves, zoning will be retained.
725
726 Figure 11. Conditions for preservation of Ti zoning in oligoclase compared with that for other
727 trace and minor elements in feldspar. Ti zoning would be better preserved than zoning of Mg and
728 Sr.
729
730 Figure 12. (**a**) Backscattered-electron image of a portion of a large K-feldspar crystal from a
731 pegmatitic vein transecting Paleoproterozoic metamorphic rocks in Colorado (N40°06.50910',
732 W105°22.34442'); exsolved albite in darker gray. The partially transparent white rectangle shows
733 the location of an LA-ICP/MS traverse across a single albite lamella ~60 microns across. (**b-f**)
734 Concentration profiles of Na, Sr, Rb, Ba and Ti along the indicated traverse. Included in (**c**) are
735 the input parameters (inset legend) and outcome (heavy lines) of moving-boundary numerical
736 models simulating albite growth and redistribution of Sr. Common to all these models are the
737 following: albite/K-feldspar partition coefficient = 0.17; initial Sr concentration in the pre-
738 exsolved feldspar = 30 ppm; total growth = 30 μm (half-width of final lamella). The uncertainty
739 in any given analysis is difficult to estimate because the data were obtained in dynamic mode as
740 the sample was translated under the laser beam in a direction perpendicular to the two-feldspar
741 interface, at a speed of 1 μm/s. We estimate the analytical uncertainty on each plotted data point
742 to be ±50% for Ti and ±20-30% for the other trace elements. The diffusivities used in the Sr
743 models are from Cherniak and Watson (1992) and Cherniak (1996), respectively. See text for
744 additional details and discussion.
745

This is a preprint, the final version is subject to change, of the American Mineralogist (MSA)
Cite as Authors (Year) Title. American Mineralogist, in press.
DOI: https://doi.org/10.2138/am-2020-7272

Figure 1

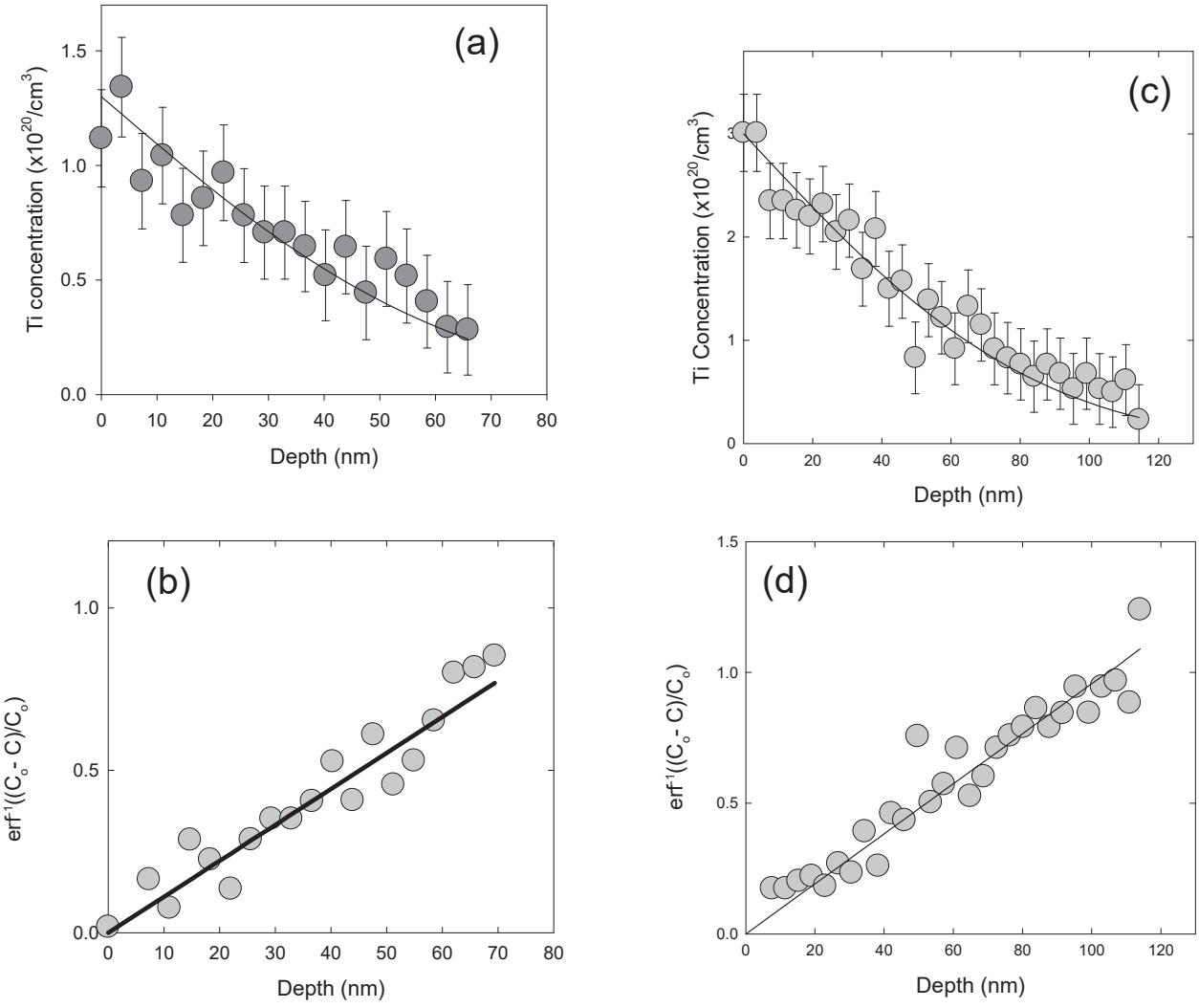

This is a preprint, the final version is subject to change, of the American Mineralogist (MSA)
Cite as Authors (Year) Title. American Mineralogist, in press.
DOI: https://doi.org/10.2138/am-2020-7272

Figure 2

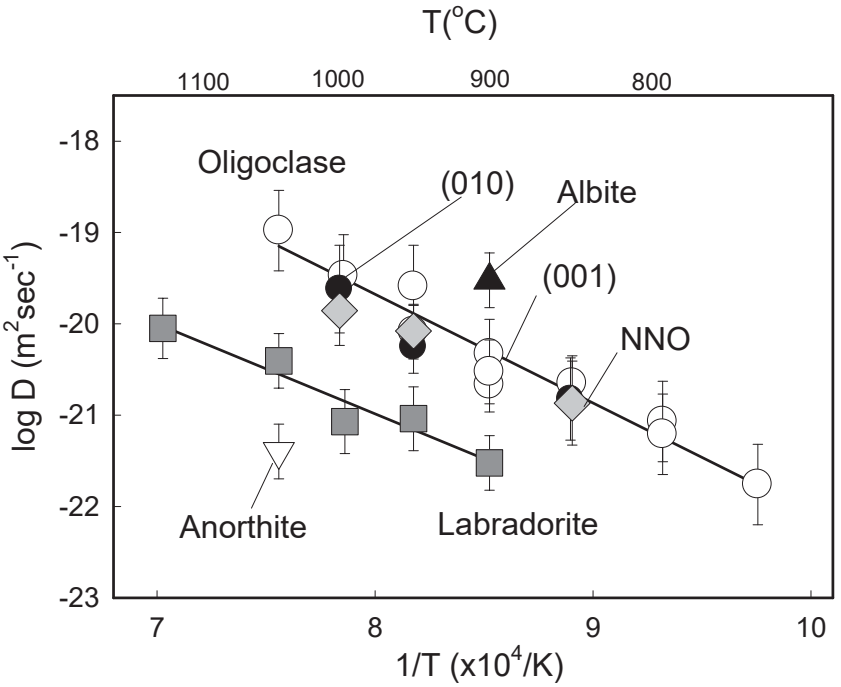

This is a preprint, the final version is subject to change, of the American Mineralogist (MSA)
Cite as Authors (Year) Title. American Mineralogist, in press.
DOI: https://doi.org/10.2138/am-2020-7272

Figure 3

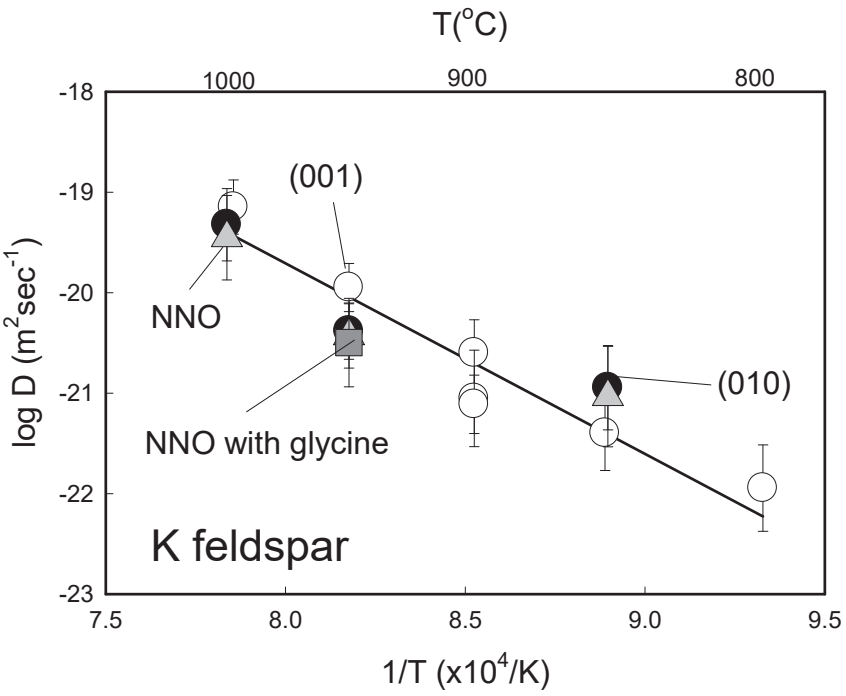

This is a preprint, the final version is subject to change, of the American Mineralogist (MSA)
Cite as Authors (Year) Title. American Mineralogist, in press.
DOI: https://doi.org/10.2138/am-2020-7272

Figure 4

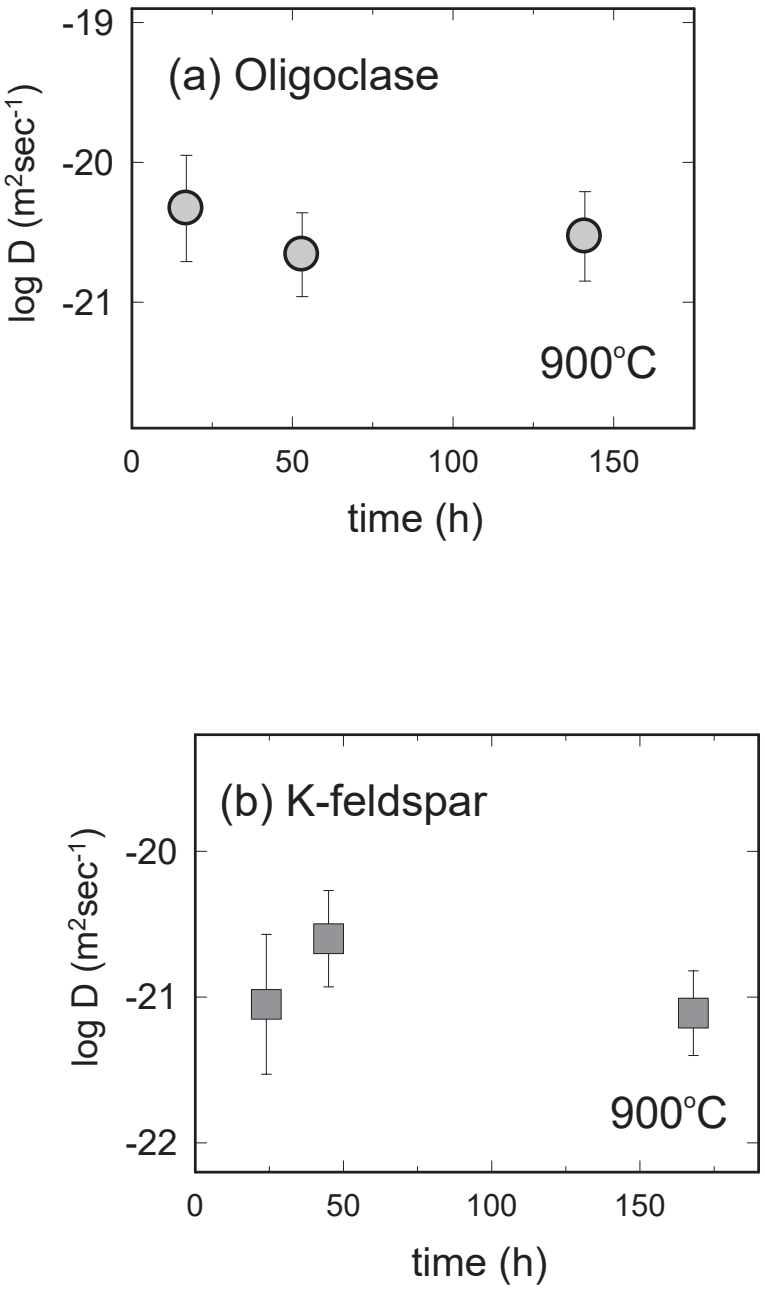

This is a preprint, the final version is subject to change, of the American Mineralogist (MSA)
Cite as Authors (Year) Title. American Mineralogist, in press.
DOI: https://doi.org/10.2138/am-2020-7272

Figure 5

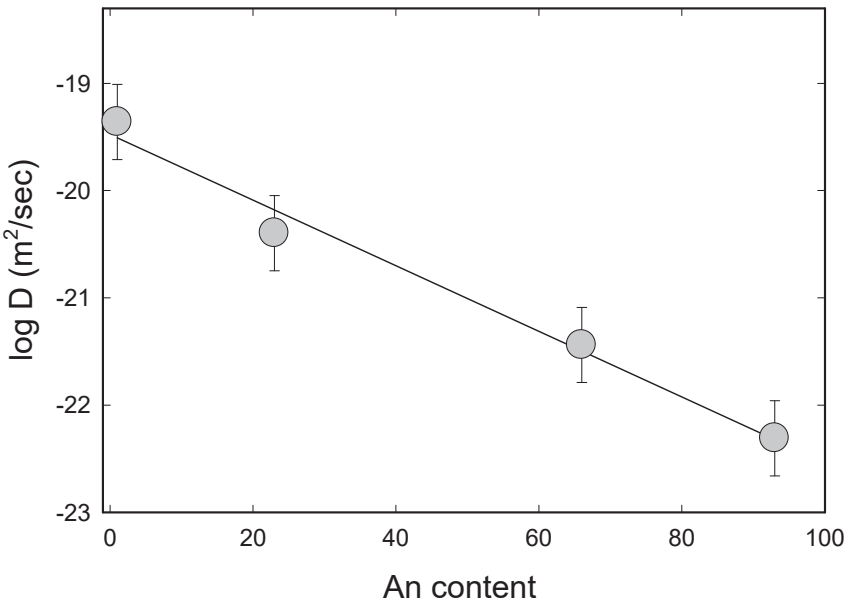

This is a preprint, the final version is subject to change, of the American Mineralogist (MSA)
Cite as Authors (Year) Title. American Mineralogist, in press.
DOI: https://doi.org/10.2138/am-2020-7272

Figure 6

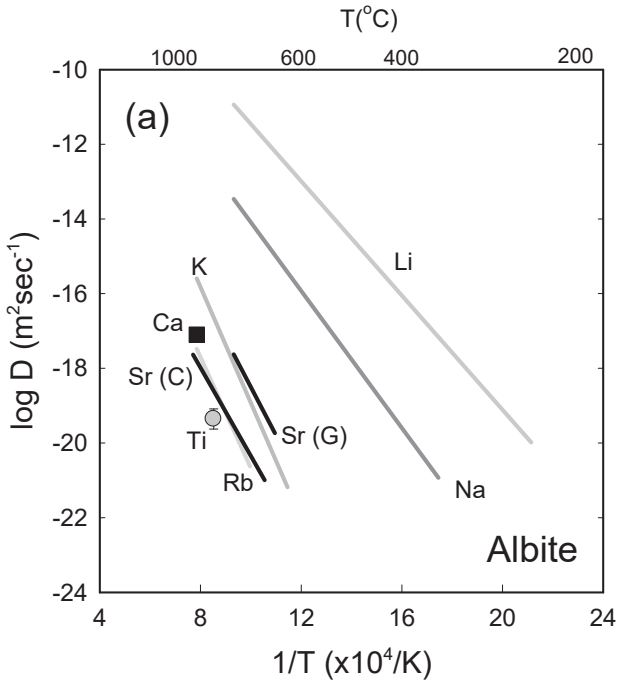

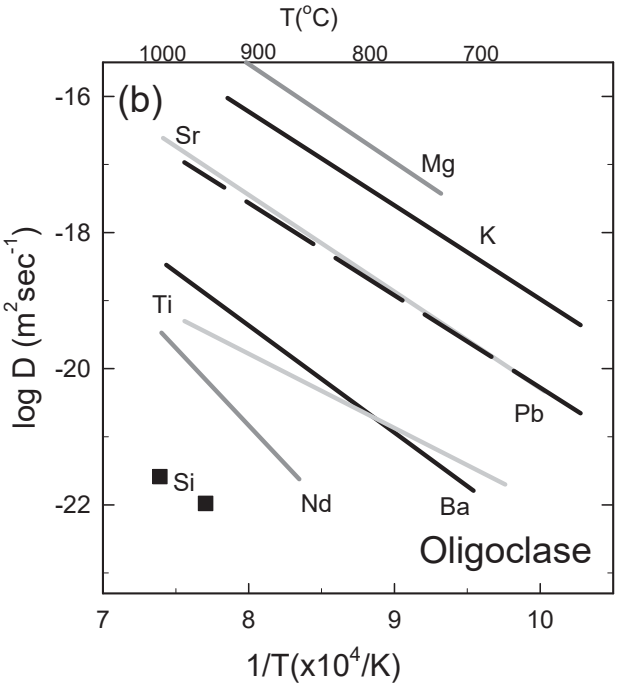

This is a preprint, the final version is subject to change, of the American Mineralogist (MSA)
Cite as Authors (Year) Title. American Mineralogist, in press.
DOI: https://doi.org/10.2138/am-2020-7272

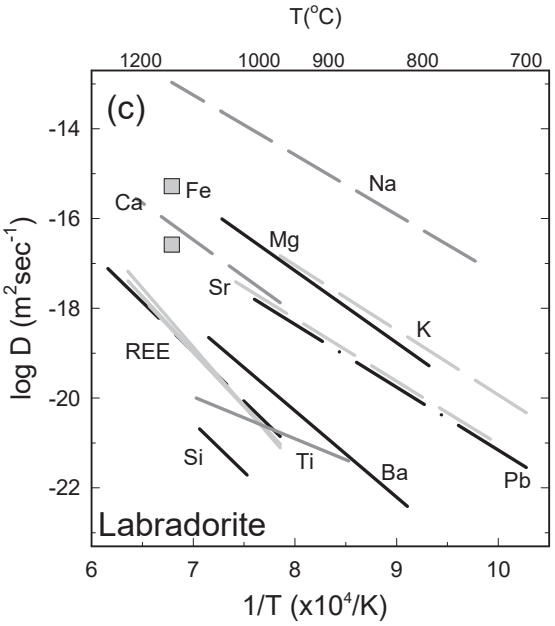

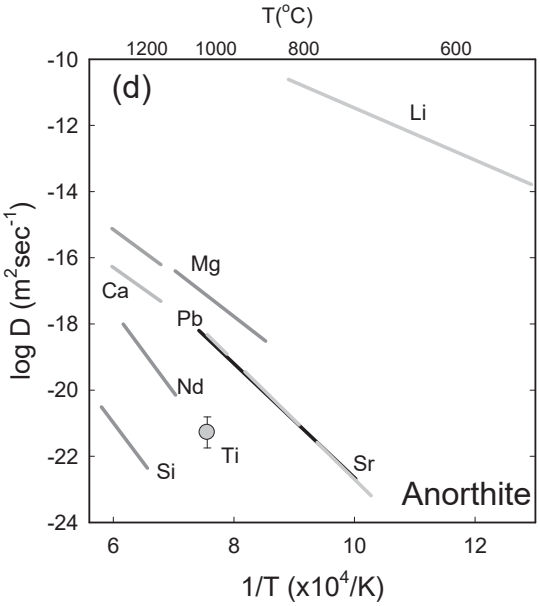

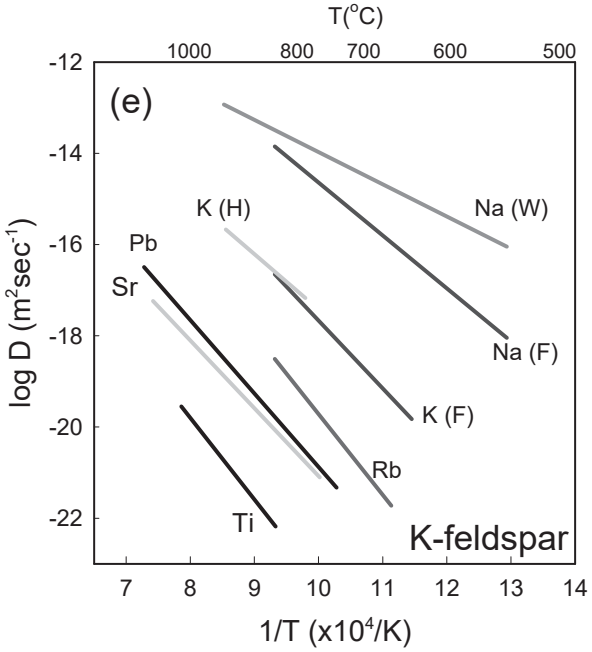

This is a preprint, the final version is subject to change, of the American Mineralogist (MSA)
Cite as Authors (Year) Title. American Mineralogist, in press.
DOI: https://doi.org/10.2138/am-2020-7272

Figure 7

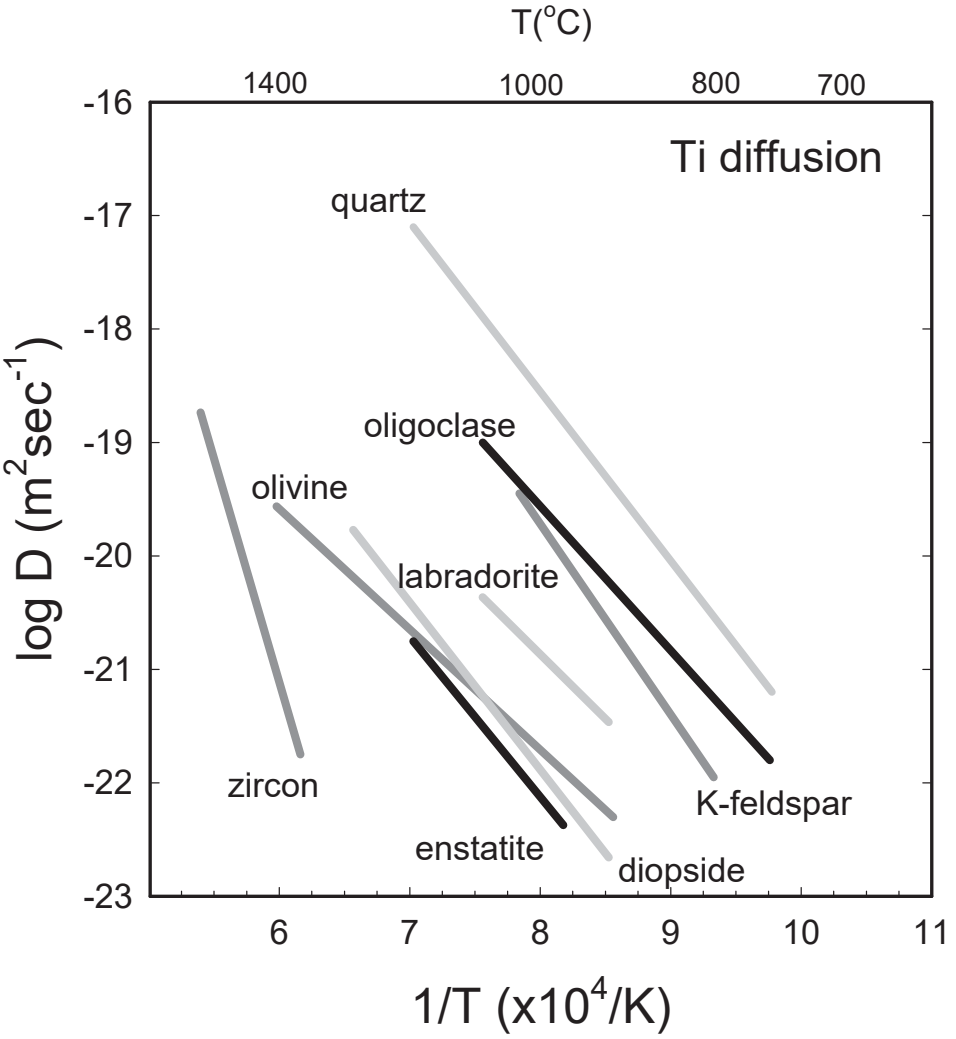

This is a preprint, the final version is subject to change, of the American Mineralogist (MSA)
Cite as Authors (Year) Title. American Mineralogist, in press.
DOI: https://doi.org/10.2138/am-2020-7272

Figure 8

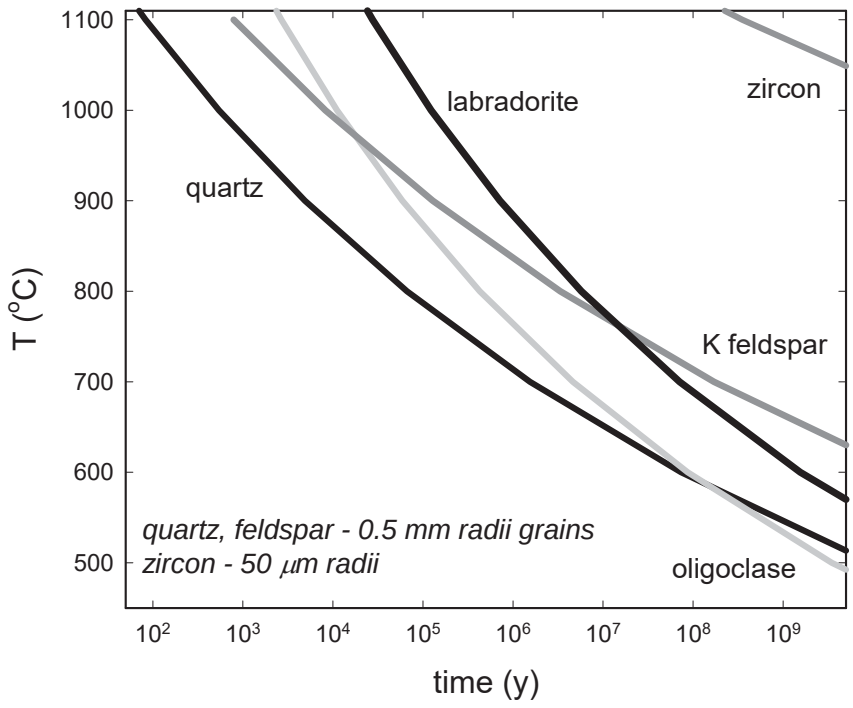

This is a preprint, the final version is subject to change, of the American Mineralogist (MSA)
Cite as Authors (Year) Title. American Mineralogist, in press.
DOI: https://doi.org/10.2138/am-2020-7272

Figure 9

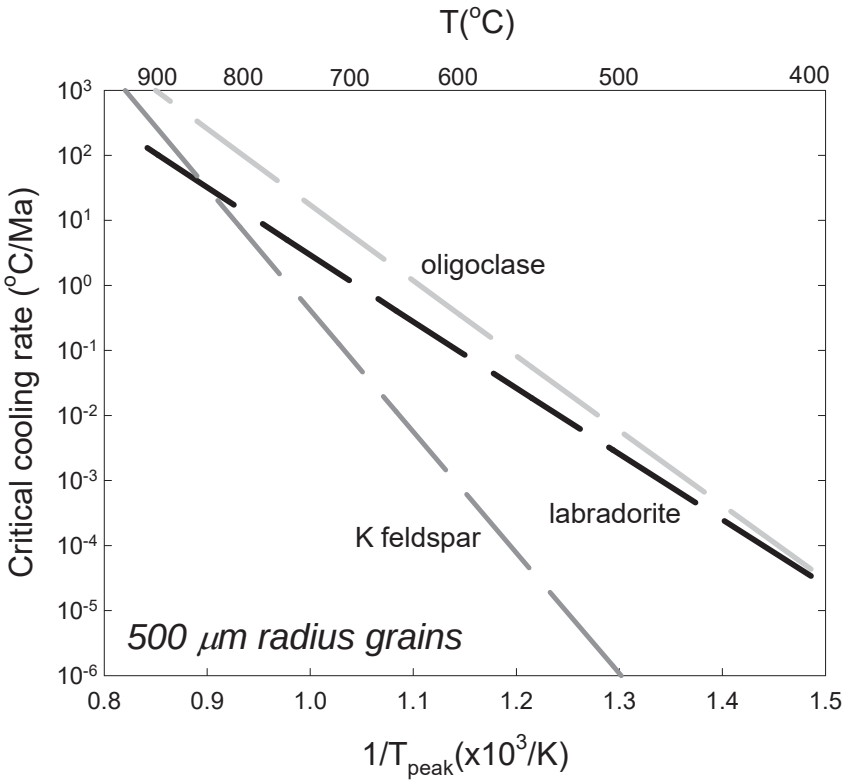

This is a preprint, the final version is subject to change, of the American Mineralogist (MSA)
Cite as Authors (Year) Title. American Mineralogist, in press.
DOI: https://doi.org/10.2138/am-2020-7272

Figure 10

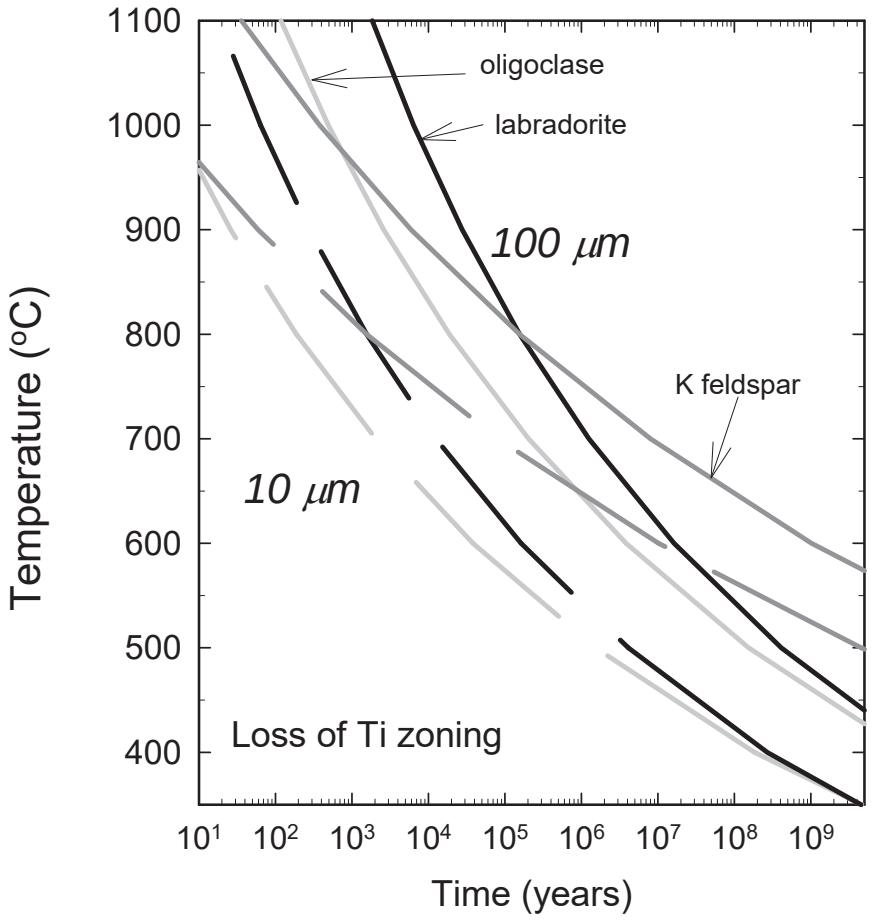

This is a preprint, the final version is subject to change, of the American Mineralogist (MSA)
Cite as Authors (Year) Title. American Mineralogist, in press.
DOI: https://doi.org/10.2138/am-2020-7272

Figure 11

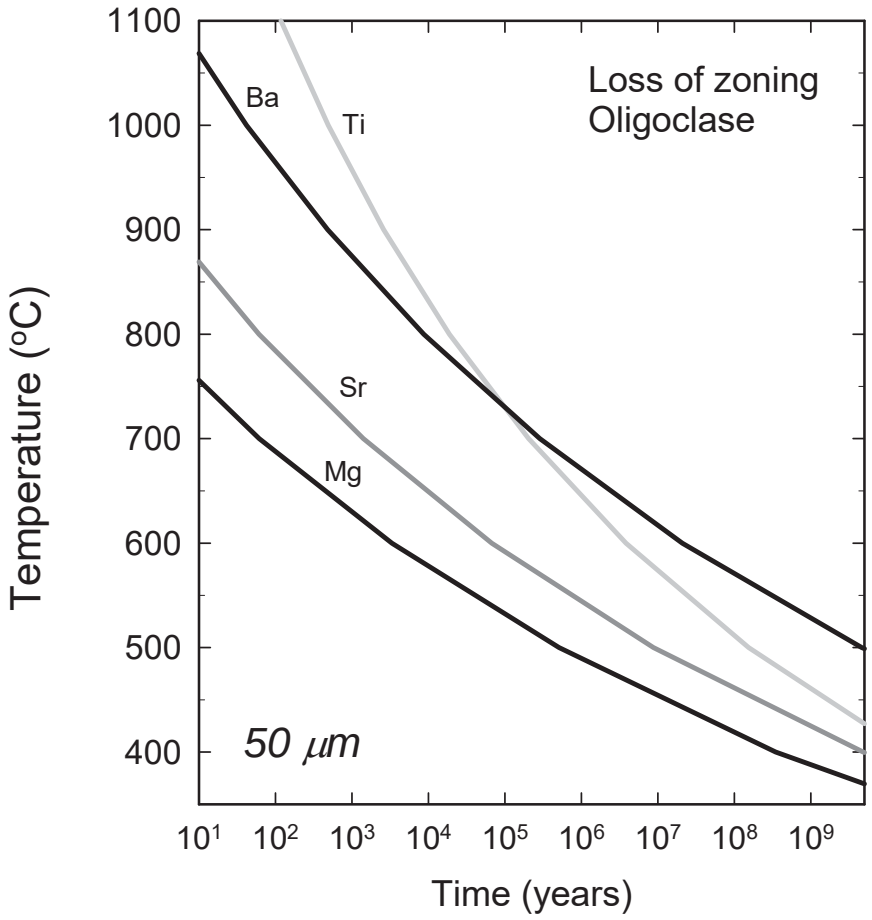

This is a preprint, the final version is subject to change, of the American Mineralogist (MSA)
Cite as Authors (Year) Title. American Mineralogist, in press.
DOI: https://doi.org/10.2138/am-2020-7272

Figure 12